Impact of sp^2 Carbon Edge Effects on the Electron Transfer Kinetics of the Ferrocene/Ferricenium Process at a Boron Doped Diamond Electrode in an Ionic Liquid

Jiezhen Li,[1] *Cameron L. Bentley,*[2] *Sze-yin Tan,*[1,2,3] *Venkata S.S. Mosalii,*[1] *Md Anisur Rahman,*[1] *Samuel J. Cobb,*[2] *Si-Xuan Guo,*[1,4] *Julie V. Macpherson,*[2] *Patrick R. Unwin,*[2] *Alan M. Bond*[1,4,*] *and Jie Zhang*[1,4,*]

[1]School of Chemistry, Monash University, Clayton, Victoria 3800, Australia

[2]Department of Chemistry, University of Warwick, Coventry, CV4 7AL, United Kingdom

[3]Department of Chemical Engineering, Imperial College London, South Kensington, London, SW7 2AZ, United Kingdom

[4]ARC Centre of Excellence for Electromaterials Science, School of Chemistry, Monash University, Clayton, Victoria 3800, Australia

Corresponding Authors

*jie.zhang@monash.edu

*alan.bond@monash.edu

Abstract. The electrochemical properties of boron doped diamond (BDD) electrodes are strongly influenced by the boron doping level and presence of sp^2 carbon impurities. In this study, the impact of highly localised sp^2 carbon concentrated at the edge of a BDD electrode, arising from laser cutting during fabrication and exposed during electrode polishing, on the resulting overall electrode kinetics is identified. Fourier transformed large amplitude alternating current (FTAC) voltammetric data for the usually ideal $Fc^{0/+}$ (Fc = ferrocene) process in the highly viscous ionic liquid 1-butyl-3-methylimidazolium hexafluorophosphate shows relatively poor agreement with simulations based on a uniformly active electrode surface, using the Butler-Volmer formalism for the electrode kinetics. In this ionic liquid medium, the impact of heterogeneity on macroscopic electrode activity is enhanced under conditions of slow mass-transport, where sites of disparate activity are spatially decoupled on the voltammetric timescale. Physically blocking this edge region leads to a response that is much more consistent with a uniform electrode and substantially improves the agreement between FTAC voltammetric experiment and simulation (standard heterogeneous electron transfer rate constant, k^0 = 0.0015 cm s^{-1}). To complement the macroscopic measurements, local voltammetric measurements with an electrochemical droplet cell show directly that the sp^2 carbon found in the edge region is able to support much faster electron transfer kinetics for the $Fc^{0/+}$ process than the sp^3 BDD surface. Overall, this study demonstrates that caution should be taken in reporting electrode kinetic data obtained at BDD electrodes, or any electrode material. Macroscopic electrode kinetic characterization in traditional electrochemical media such as acetonitrile are blind to such heterogeneities in activity. However, tuning the diffusional timescale through the use of FTAC voltammetry in viscous ionic liquids provides a powerful approach for detecting spatially non-uniform electrode activity.

INTRODUCTION

sp^2 carbon materials such as glassy carbon (GC) and pyrolytic graphite are widely used as electrodes in dynamic electrochemistry (voltammetry), as they exhibit wider electrochemical potential windows than metals.[1] However, these materials may also possess some intrinsic disadvantages, such as relatively high background capacitance current resulting from a combination of porosity and the presence of edge plane graphite-like layers, as well as a propensity for surface functionalization/fouling.[2-3] In contrast, the completely sp^3 hybridized, tetrahedral bonding of diamond, in its boron-doped form, retains the traditional advantages of carbon electrode materials such as a wide electrochemical window, with the benefit of very low double layer capacitance, as well as higher chemical inertness and thermal conductivity.[4-6]

Boron doped diamond (BDD) is used for electrochemical applications predominantly in the polycrystalline form. It has been reported that the electrochemical behaviour of BDD may be influenced by factors such as: (i) boron doping level, (ii) morphological features such as grain boundaries and point defects, (iii) sp^2 carbon impurity content, (iv) crystallographic orientation, and (v) surface functional groups (such as H, O, F, *etc*.).[7-8] The boron doping level on BDD is facet-dependent, due to facet-dependent variations in dopant density and surface termination. Thus, the electron transfer kinetics at the reversible potential (heterogeneous electron transfer rate constant, k^0) on BDD is governed by the local boron dopant concentration;[9-11] exposed surface facets with higher boron content have higher k^0 values. Consequently, the bulk (macroscopic) voltammetric response of a BDD electrode depends on the heterogeneity of boron doping and the doping level, and associated non-uniform diffusion to individual facets. The overall measured response is thus a complex function of the facet size and spatial distribution across the electrode, the diffusion coefficient of the electroactive species and the time scale of the experiment.[12-13]

The presence of non-diamond sp^2 carbon impurities also can have a significant impact on electrochemical kinetics at BDD electrodes as well as resulting in a reduced electrochemical potential window and enhanced background (capacitive) currents.[14-15] In aqueous media, the presence of sp^2 carbon impurities was found to increase the electron transfer kinetics of inner sphere processes (4-tert-butylcatechol oxidation), while having minimal influence on outer sphere ones ($Ru(NH_3)_6^{3+/2+}$ reduction).[14] sp^2 carbon impurity has also been suggested to act as a charge transfer mediator for the 1,4-benzoquinone/hydroquinone couple.[16] From these literature reports, it is clear that sp^2 carbon is an important factor that affects the electrochemical behaviour of BDD electrodes.

sp^2 carbon impurities are commonly introduced during chemical vapour deposition growth of the BDD, with the highest concentration likely to be present at grain boundaries.[6] For ultra-nanocrystalline (grain size < 10 nm) and nanocrystalline (grain sizes in the range 10 nm – 1 μm) BDD, due to the growth conditions employed[6] and the fact that the grain boundary density is substantial, the presence of sp^2 carbon is particularly significant.[17-18] Nevertheless, by optimizing the deposition conditions, it is possible to grow high-quality microcrystalline (grain sizes > 1μm) BDD with negligible sp^2 carbon content.[19-20]

Two experimental setups are commonly employed in studies of BDD electrodes. In one format, the cell body is attached to the front face of the BDD electrode, which is larger in size than the electrochemical cell. Alternatively, the BDD is cut to the appropriate electrode geometry and then sealed around the edges using an insulator.[6] Cutting BDD requires a laser micromachining process,[21] which results in the introduction of sp^2 carbon impurities down the sidewalls of the freestanding BDD. Ideally, the edge region will be fully sealed in an insulating material (*e.g.*, glass) resulting in a co-planar arrangement but inevitably, especially with repeated usage and cleaning, the sp^2 rich region will progressively become more exposed, a feature that is in detail herein. Laser micromachining has also been used to controllably

introduce sp^2 carbon into the BDD surface[22] to increase its electrocatalytic activity to oxygen reduction[23] and introduce quinone functional groups for use in pH sensing.[24]

Historically, electrochemical theory was tested experimentally using well-defined mercury electrodes, where an ideal homogeneous surface is readily available. However, the solid electrodes widely used in modern electrochemical science, particularly those that are carbon-based, usually have heterogeneous surfaces.[10, 25-26] Detailed studies[27-30] have demonstrated that surface inhomogeneity may introduce significant non-ideal behavior relative to that predicted for a homogeneous surface. In a recent study from this laboratory,[31] it was demonstrated that Fourier-transformed large amplitude alternating current (FTAC) voltammetry is far more sensitive than conventional direct current, DC, voltammetric methods for quantifying electron transfer kinetics at disparately active electrode surfaces. In studies with a model GC and BDD electrode configuration, the active sites were spatially separated and macroscopic. In this model system, the FTAC voltammetric response deviated significantly from the theory based on a simple homogeneous surface. In particular, the harmonic-dependent kinetic sensitivity of FTAC voltammetry allowed the heterogeneous rate constants at both GC and BDD electrodes to be resolved and quantified from the signal resulting from a simultaneous measurement of the two electrodes.

Herein, FTAC voltammetry was applied to probe the electrode kinetics of the $Fc^{0/+}$ (Fc = ferrocene) process at a BDD electrode in the highly viscous ionic liquid (IL) 1-butyl-3-methylimidazolium hexafluorophosphate, [BMIM][PF_6] (viscosity, η = 294 cP at 22ºC).[32] $Fc^{0/+}$ is nominally an ideal, simple and rapid one electron process in many traditional solvent/electrolyte media as well as [BMIM][PF_6], at both metal and GC electrodes. Contrary to previous studies,[33-34] in this work the experimental data presented herein were found to deviate significantly from those predicted theoretically using the traditional Butler-Volmer model of electron transfer. In-depth investigations revealed a sp^2 carbon-rich edge region of

the BDD disc (extruded from the electrode sealing due to polishing) to be the origin of the discrepancy. Kinetic deviation is exacerbated in this highly viscous ionic liquid due to the small diffusion coefficient of Fc (*ca.* 10^{-8} cm^2 s^{-1}), which minimises overlap of diffusion in the sp^2 rich edge and very low sp^2 level areas on the face of the electrode on the FTAC voltammetric timescale.

EXPERIMENTAL SECTION

Chemicals. 1-butyl-3-methylimidazolium hexafluorophosphate ([BMIM][PF_6], Io-li-tec) was dried by purging with dry N_2 for 48 hours.[35] Acetonitrile (CH_3CN, 99.9%, Sigma-Aldrich), was used as supplied by the manufacturer. Tetrabutylammonium hexafluorophosphate ([TBA][PF_6], 98%, Wako) was recrystallized twice from ethanol (96%, Merck) before use as the supporting electrolyte in acetonitrile. Ferrocene (Fc, Sigma-Aldrich, ≥ 98 %) was recrystallized from *n*-pentane (Merck, EMSURE).

Electrode fabrication. Glass sealed BDD electrodes were fabricated as previously reported.[21] For localized electrochemical droplet cell measurements, a 400 µm diameter disk shaped feature was machined in a BDD plate of negligible sp^2 content[8] using a 355 nm frequency tripled Nd:YAG 34 ns laser micromachiner (E-355H-ATHI-O system, Oxford Lasers) at a pulse density of 2×10^6 cm^{-2} and pulse fluence of 870 J cm^{-2}. Once machined, the electrodes were acid treated in boiling concentrated H_2SO_4 (98%) saturated with KNO_3 to oxygen-terminate the surface. To provide a reliable ohmic contact, Ti (10 nm)/Au (300 nm) was sputtered (MiniLab 060 Platform, Moorfield Nanotechnology Ltd.) onto the back face and annealed at 400 °C for 5 h.[8]

Electrochemical instrumentation and procedures. DC cyclic voltammetric experiments were carried out with a CHI 760E electrochemical workstation (CH Instruments, USA). FTAC voltammetric experiments were undertaken with home-built instrumentation,[36] using a sinusoidal wave perturbation with an amplitude, ΔE, of 80 mV and frequency, f, of 9.02 Hz,

26.97 Hz or 80.99 Hz superimposed onto a DC ramp with a scan rate, υ. After data collection, the total DC plus AC current was subjected to Fourier transformation to obtain the power spectrum. After selection of the frequency band of interest, inverse Fourier transformation was used to generate the required aperiodic DC or AC harmonic components.[36-38]

A standard three-electrode cell configuration was used for all electrochemical experiments, which were undertaken at room temperature (22 ± 2°C) inside a glove box to minimize the influence of water and oxygen. The working electrodes were glassy carbon (nominal diameter, *d*, = 1.0 mm) or glass sealed oxygen-terminated, polycrystalline BDD (constructed as described above, *d* = 1.0 mm).[20] The boron concentration of the BDD sample was ~3×10^{20} atoms cm^{-3} (average), which is above the metallic threshold.[20] Platinum wire was used as both the auxiliary and reference electrode. The electrode potential for the $Fc^{0/+}$ process was set at 0 V as recommended by IUPAC.[39] Prior to each voltammetric experiment, the working electrode was polished with an aqueous 0.05 μm alumina slurry on a clean polishing cloth, rinsed with water then acetone, and finally dried under nitrogen. The electrochemically active area, *A*, of the working electrodes were calculated from analysis of a plot of the DC peak current versus the square root of scan rate for the reversible oxidation of 1.0 mM Fc in CH_3CN (0.1 M [TBA][PF_6]) using the Randles-Sevcik relationship[40] and the known diffusion coefficient, *D*, of 2.4×10^{-5} cm^2 s^{-1} for Fc.[41] The areas of the GC and BDD electrodes determined in this manner were 7.9×10^{-3} and 7.7×10^{-3} cm^2, respectively, which are close to values expected based on the nominal electrode diameters (≈7.85×10^{-3} cm^2).

Electrochemical droplet cell measurements. Local electrochemical (cyclic voltammetric) measurements were carried out in the electrochemical droplet cell format, as previously reported.[42-43] In brief, a single barrel micropipette was pulled to ≈50 μm tapered end, filled with 3.4 mM Fc in [BMIM][PF_6] and mounted on a *z*-piezoelectric positioner (P-753.3CD, PhysikInstrumente). A piece of freestanding polycrystalline BDD that possessed a disk-shaped

area of sp^2-rich material (introduced by laser micromachining, *vide supra*) served as the working electrode substrate, which was mounted on *xy*-micropositioners and positioned below the micropipet probe. After positioning the micropipet probe above the surface-region of interest (achieved using a PL-B776U Camera equipped with a 6× lens, Pixelink, U.S.A.), it was approached to the surface at a constant rate (5 μm/s) using the *z*-piezoelectric positioner until meniscus (droplet) contact was made (note that the micropipet itself did not make contact with the surface). During approach, a potential bias was applied between the conducting substrate and a quasi-reference counter electrode (Pt wire) that was located within the barrel of the micropipet, and the current that flowed when meniscus contact was initially made when closing the electrochemical circuit served as a feedback signal to halt the approach. Cyclic voltammetry measurements were performed in the confined area defined by the contact between the electrolyte droplet cell and substrate surface. A two-electrode cell could be used due to the small currents measured (pA range) (*vide infra*).

Preparation of BDD wax insulated electrode. The details of the *BDD wax insulated electrode* preparation and its configuration can be found in Supporting Information (SI) and Figure S1.

Other instrumentation. Raman spectroscopy was conducted using a Renishaw InVia Raman spectrometer with a laser excitation at 488 nm. Optical microscopy images were obtained using a Nikon Eclipse Ni optical microscope.

Theory-experiment comparison. Since negligible differences are expected between Butler-Volmer (BV) and Marcus-Hush theories in simulations when the electron transfer kinetics are relatively fast, as applies to the $Fc^{0/+}$ process studied in this paper,[44] the simpler BV theory was used in all simulations. Simulating the simple one-electron transfer reaction given in Equation (1),

$$R \rightleftharpoons O + e^- \quad (E_f^0, k^0, \alpha) \qquad (1)$$

requires six parameters: formal reversible potential, E_f^0, heterogeneous electron transfer rate constant, k^0, charge transfer coefficient, α, diffusion coefficient, D, uncompensated resistance, R_u, and capacitance, C_{dl}.

R_u and C_{dl} were estimated from the background current in the fundamental harmonic at potentials where faradaic current is absent. In order to define the potential dependence of C_{dl}, a nonlinear capacitor model was used, as described elsewhere:[45]

$$C_{dl}(t) = C_0 + C_1E(t) + C_2E(t)^2 + C_3E(t)^3 + C_4E(t)^4 \qquad (2)$$

The R_u value was estimated experimentally from the *RC* time constant and AC impedance methods[32] available with the CHI instrument. E_f^0 was defined as 0 V vs $Fc^{0/+}$ in all simulations. D_{Fc} was calculated from the magnitude of the oxidation peak current at a bare GC electrode and was found to be 6.3×10^{-8} cm s^{-1}, as described in the SI. Despite reports of $D_{Fc^+} \neq D_{Fc}$ in [BMIM][PF_6], ($D_{Fc} = 5.9 \times 10^{-8}$ cm^2 s^{-1} *vs.* $D_{Fc^+} = 3.1 \times 10^{-8}$ cm^2 s^{-1}),[33] in all FTAC voltammetric simulations reported herein, it was assumed that $D_{Fc^+} = D_{Fc}$ for simplicity since the difference only affects the formal reversible potential and has a negligible effect on electrode kinetics parameters. α was assumed to be 0.50, which is reasonable for the outer sphere $Fc^{0/+}$ process. Under these circumstances, the only unknown parameter that needs to be derived from experiment-simulation comparisons is k^0.

The method used for comparison of experimental and MECSim simulated data adopted here is described elsewhere.[46] Firstly, MECSim software is scripted to cover a wide range of k^0 values with total current versus time data generated for each set of parameters. Next, a least-squares (LS) comparison of experimental and simulated total current versus time data is undertaken for each parameter set. Finally, by combining the LS correlation comparisons, a map of quality of agreement as a function of parameters being estimated is obtained from which the best fit generated in the parameter optimization exercise is derived.

The LS correlation used to quantify the agreement between experimental and simulated data is given by:

$$LS = \left[1 - \frac{1}{H+1}\left(\sum_{h=0}^{H}\sqrt{\frac{\sum_{i=1}^{N}[(f_h^{exp}(x_i) - f_h^{sim}(x_i))^2]}{\sum_{i=1}^{N} f_h^{exp}(x_i)^2}}\right)\right] \times 100\% \qquad (3)$$

where $f^{exp}(x_i)$ and $f^{sim}(x_i)$ are the experimental and simulated functions, respectively, h represents aperiodic DC when h = 0 or the AC harmonic component when k = 1 to H, H is the total number of AC harmonic components and N is the number of data points. An LS value of 100% will be obtained if perfect agreement between experimental and simulated data is achieved. In the present study, the aperiodic DC and up to 6 AC harmonic components were used for the LS calculation. Finally, it should be noted that the first and last second of the FTAC voltammetric data set were omitted from the LS calculation because they are dominated by "ringing" noise.

RESULTS AND DISCUSSION

FTAC voltammetric analysis of the $Fc^{0/+}$ process in [BMIM][PF_6] at a BDD electrode. In [BMIM][PF_6], Fc undergoes a one-electron oxidation process:

$$Fc \rightleftharpoons Fc^+ + e^- \qquad (4)$$

In order to extract the k^0 value for the $Fc^{0/+}$ process at a BDD electrode in [BMIM][PF_6], FTAC voltammetric studies were carried out using a sine wave perturbation of ΔE = 80 mV with f = 9.02, 26.97 or 80.99 Hz. Figure 1 provides experimental data along with simulations and computationally derived best fit values at a frequency of 9.02 Hz. Relatively poor agreement between theory and experiment was obtained, with the optimized k^0 value of 0.0023 cm s^{-1} having a LS value of 83.2%. Specifically, the simulated data only fit well with the experimental data at the aperiodic DC and 4th AC harmonic components, while the current magnitude overestimated and underestimated for lower and higher harmonics, respectively. Moreover, an

increasing level of discrepancy between experimental and simulated data was observed when higher frequencies of 26.97 and 80.99 Hz were used, respectively as shown in Figures S2 and S3, with LS values calculated to be 74.0 % and 66.7 %, respectively. Thus, the k^0 value is apparently harmonic (timescale) dependent, which is physically meaningless, leading to the conclusion that the electrode reaction mechanism is more complex than assumed in the simulation model.

FTAC voltammetric data were also collected at a 2-fold lower Fc concentration (SI, Figures S4 – S6). A similar level of deviation between the experimental and simulated data was observed at with a Fc concentration of 0.5 mM. The apparent k^0 and LS values obtained at a BDD electrode for the $Fc^{0/+}$ process with bulk Fc concentrations of 1.0 and 0.5 mM are summarized in Table 1. The concentration independent results imply that the experiment-simulation discrepancy is not due to the presence of second or higher order reactions, an adsorption effect or an IR_u effect.

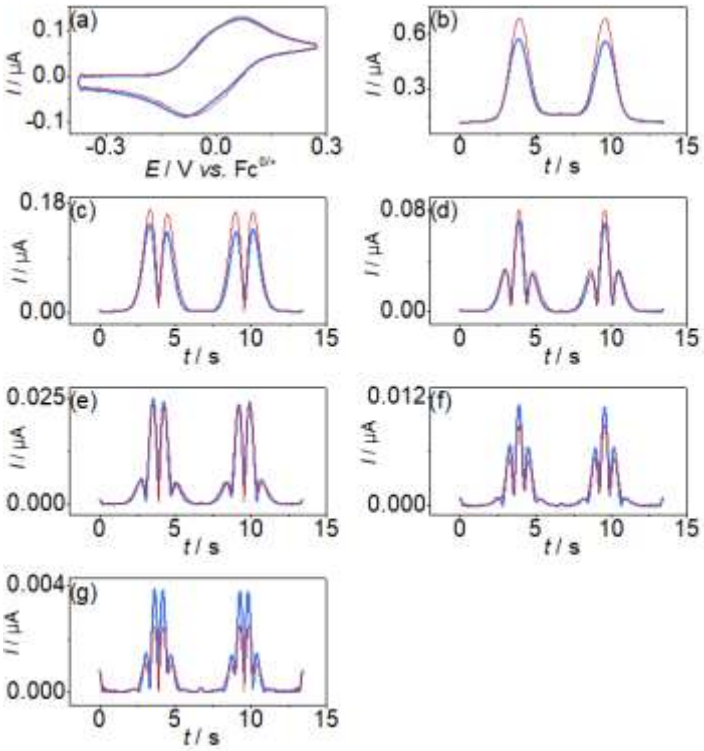

Figure 1. Comparison of simulated (red) and experimental (blue) FTAC voltammetric data obtained from the oxidation of 1.0 mM Fc in [BMIM][PF_6] at a BDD macrodisk electrode with ΔE = 80 mV, f = 9.02 Hz and v = 0.087 V s^{-1}. (a) aperiodic DC component, (b-g) 1st to 6th AC harmonic components. The simulation parameters

are $A = 7.7 \times 10^{-3}$ cm^2, $D = 6.3 \times 10^{-8}$ cm^2 s^{-1}, $R_u = 3338$ Ω, $E^0 = 0$ V *vs.* $Fc^{0/+}$, C_{dl} ($C_0 = 3.4$, $C_1 = 0.8$, $C_2 = 1.0$, $C_3 = 0.7$, $C_4 = -2.2$) μF cm^{-2} (see eq 2), $T = 295$ K, $k^0 = 0.0023$ cm s^{-1} and $a = 0.50$. LS = 83.2 %.

Table 1 Comparison of k^0 values derived from experiment versus simulation comparison of $Fc^{0/+}$ processes in [BMIM][PF_6] at GC and BDD electrodes.

	BDD						GC					
D	9.02 Hz		26.97 Hz		80.99 Hz		9.02 Hz		26.97 Hz		80.99 Hz	
	k^0 (cm s^{-1})	LS (%)	k^0 (cm s^{-1})	LS (%)	k^0 (cm s^{-1})	LS (%)	k^0 (cm s^{-1})	LS (%)	k^0 (cm s^{-1})	LS (%)	k^0 (cm s^{-1})	LS (%)
1.0 mM	0.0023	83.2	0.0025	74.0	0.0025	66.7	≥ 0.030	93.6	0.040	95.4	0.040	92.5
0.50 mM	0.0025	82.9	0.0031	74.6	0.0055	59.1	≥ 0.030	95.9	0.035	94.9	0.040	93.4

FTAC voltammetric analysis of the $Fc^{0/+}$ process in acetonitrile at a BDD electrode. A number of reports have described the DC voltammetry of the $Fc^{0/+}$ couple in acetonitrile at a BDD electrode.[47-49] In all cases, well defined cyclic voltammograms were observed and k^0 values were determined to be in the low to mid 10^{-2} cm s^{-1} range. In this study, FTAC voltammetry was used to examine the electrode kinetics of the $Fc^{0/+}$ process in acetonitrile at the BDD electrode. As shown in Figure 2, with use of a frequency of 26.97 Hz, excellent experiment-theory agreement was obtained (LS = 94.8 %) at the BDD electrode for the 1st to 6th harmonics, with the majority of discrepancy in the aperiodic DC component being attributable radial diffusion contributions to the overall mass transport (Figure S7 and relevant discussion in Supporting Information for further details). From this simulation-experiment comparison, the k^0 value is estimated to be 0.085 cm s^{-1} for the BDD electrode, which is broadly in agreement with that reported in the literature of 0.048 cm s^{-1} using a hydrogen-terminated BDD electrode with a boron doping density in the mid 10^{19} to low 10^{20} atom cm^{-3} range.[47]

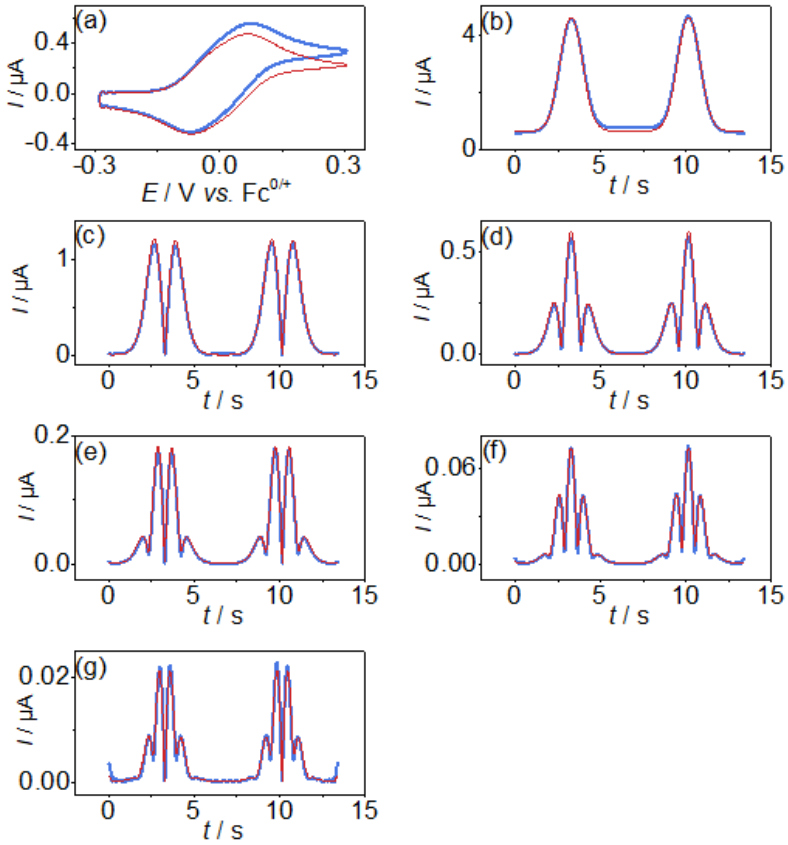

Figure 2. Comparison of simulated (red) and experimental (blue) FTAC voltammetric data obtained from the oxidation of 0.20 mM Fc in CH_3CN (0.10 M [TBA][PF_6]) at a BDD macrodisk electrode with ΔE = 80 mV, f = 26.97 Hz and v = 0.089 V s^{-1}. (a) aperiodic DC component, (b-g) 1st to 6th AC harmonic components. The simulation parameters are $A = 7.7 \times 10^{-3}$ cm^2, $D = 2.4 \times 10^{-5}$ cm^2 s^{-1}, R_u = 430 Ω, E^0 = 0 V *vs.* $Fc^{0/+}$, C_{dl} (C_0 = 6.0 µF cm^{-2}) (see eq 2), T = 295 K, k^0 = 0.085 cm s^{-1} and a = 0.50. LS = 94.8 %.

FTAC voltammetric analysis of the $Fc^{0/+}$ process in [BMIM][PF_6] at a GC electrode. Even though GC electrodes may contain a variety of surface functional groups such as carboxylates,[50] quinones,[51] phenols,[51] as determined by the surface treatment, the scale of the heterogeneities are usually very small compared to the diffusion length (*i.e.*, the surface is microstructurally isotropic), giving rise to homogeneous electrochemical activity.[52-53] Thus, FTAC voltammetric studies at a GC electrode for the $Fc^{0/+}$ process in [BMIM][PF_6] provided far better agreement between experimental and simulated data than for the BDD case. Frequencies of 9.02 Hz (Figure 3), 26.97 Hz (SI, Figure S8) and 80.99 Hz (SI, Figure S9), give rise to LS values of 93.6%, 95.4% and 92.5% and k^0 values of ≥ 0.030 cm s^{-1}, 0.040 cm s^{-1} and 0.040 cm s^{-1}, respectively. FTAC voltammetric data obtained for the oxidation of 0.50 mM Fc

in[BMIM][PF_6] also achieved excellent agreements between the simulated and experimental data at a GC electrode for all frequencies studied (see SI, Figures S10 to S12). The k^0 and LS values obtained at a GC electrode for the $Fc^{0/+}$ process at 1.0 and 0.50 mM concentrations are summarized in Table 1. The substantially improved agreement between theoretical and experimental data at the GC electrode in [BMIM][PF_6] further reiterates the enhanced influence of surface heterogeneity on the FTAC voltammetric response at BDD above (see Figure 1). The nature of the heterogeneity that gives rise to the apparently frequency-dependent k^0 values (kinetic dispersion) at BDD is explored in detail below.

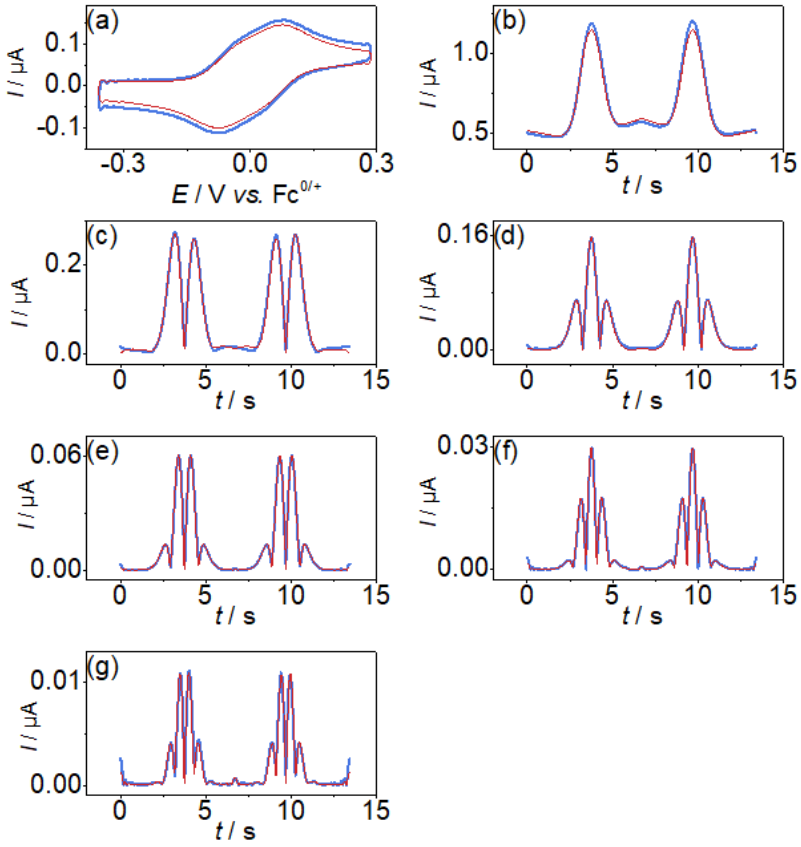

Figure 3. Comparison of simulated (red) and experimental (blue) FTAC voltammetric data obtained from the oxidation of 1.0 mM Fc in [BMIM][PF_6] at a GC macrodisk electrode with ΔE = 80 mV, f = 9.02 Hz and v = 0.087 V s^{-1}. (a) aperiodic DC component, (b-g) 1st to 6th AC harmonic components. The simulation parameters are $A = 7.9 \times 10^{-3}$ cm^2, $D = 6.3 \times 10^{-8}$ cm^2 s^{-1}, R_u = 3638 Ω, E^0 = 0 V *vs.* $Fc^{0/+}$, C_{dl} (C_0 = 13.2, C_1 = −2.2, C_2 = 8.5, C_3 = 13.9, C_4 = −24.0) μF cm^{-2} (see eq 2), T = 295 K, $k^0 \geq 0.030$ cm s^{-1} and a = 0.50. LS = 93.6 %.

Origins of the discrepancy between the experimental and simulated FTAC voltammetric data in [BMIM][PF_6] at the BDD electrode. The discrepancy between the experimental and

simulated FTAC voltammetric data in [BMIM][PF_6] in principle could be due to the kinetic dispersion arising from the large grain size coupled with grain-dependent k^0 values,[9-10] as illustrated in Figure 4. Figure 4a shows an SEM image of the BDD electrode surface, which is structurally heterogeneous (polycrystalline) electrode with individual grains ~20 μm in size containing variable levels of boron doping as evidenced by the contrast visible in the image. As alluded above, the voltammetric behaviour of the BDD electrode is the net effect of the activity of each individual facet and the scale of the spatial heterogeneity compared to the overall size of the diffusion layer. Thus, the distribution of facet size and their intrinsic activities, the diffusion coefficient of the electroactive species and the time scale of the experiment are critical in determining the overall voltammetric response. For instance, for large grain sizes and compressed diffusion layers favored by short timescales or low diffusion coefficients, overlap of diffusion layers associated with individual facets is expected to be minimal allowing the electrode to behave as a heterogeneous surface. Conversely, for small grain sizes and expanded diffusion layers favored by long timescales or large diffusion coefficients, the diffusion layers associated with individual facets overlap extensively and the linear diffusion model of mass transport applies, which translates to the behaviours associated with a homogeneous electrode surface.

An important difference between acetonitrile and [BMIM][PF_6] media is that the viscosity of the former is ≈10^3 times smaller than the latter ($\eta_{CH_3CN} = 0.48$ cP and $\eta_{[BMIM][PF_6]} = 294$ cP).[32] In voltammetry, the concentration of electroactive species deviates from bulk concentration within the diffusion length (δ) of $6\sqrt{Dt}$ from the electrode surface.[40] Therefore, in low viscosity acetonitrile, the diffusion layers adjacent to the low and high activity domains overlap significantly even on a relatively short timescale associated with the 6th harmonic (i.e. $t = 1/(9 \times 6) = 0.019$ s) based on the calculation summarized in Table 2. As a result, the FTAC voltammetric data can be approximately described by the theory based on

a homogeneous surface and linear diffusion (Figure 4b). By contrast, in viscous [BMIM][PF_6], the low value of D_{Fc} (*ca.* 6.3×10^{-8} cm^2 s^{-1}) results in much more compressed diffusion layers (as shown in Table 2) and thus much less overlap of the diffusion layers occurs on the experimental timescale (*e.g.*, Figure 4c). As a result, a frequency and harmonic dependent k^0 value is expected in FTAC voltammetric response due to the high kinetic sensitivity associated with this technique.[54]

Table 2 Thickness of diffusion layers of Fc in acetonitrile and [BMIM][PF_6], at measurement time scales corresponding to first to sixth harmonic components in FTAC voltammetry, at a frequency of 9 Hz.

harmonic	1st	2nd	3rd	4th	5th	6th
δ_{CH3CN} (μm)	95.9	67.8	55.4	48.0	42.9	39.2
$\delta_{[BMIM][PF6]}$ (μm)	5.0	3.6	2.9	2.5	2.2	2.1

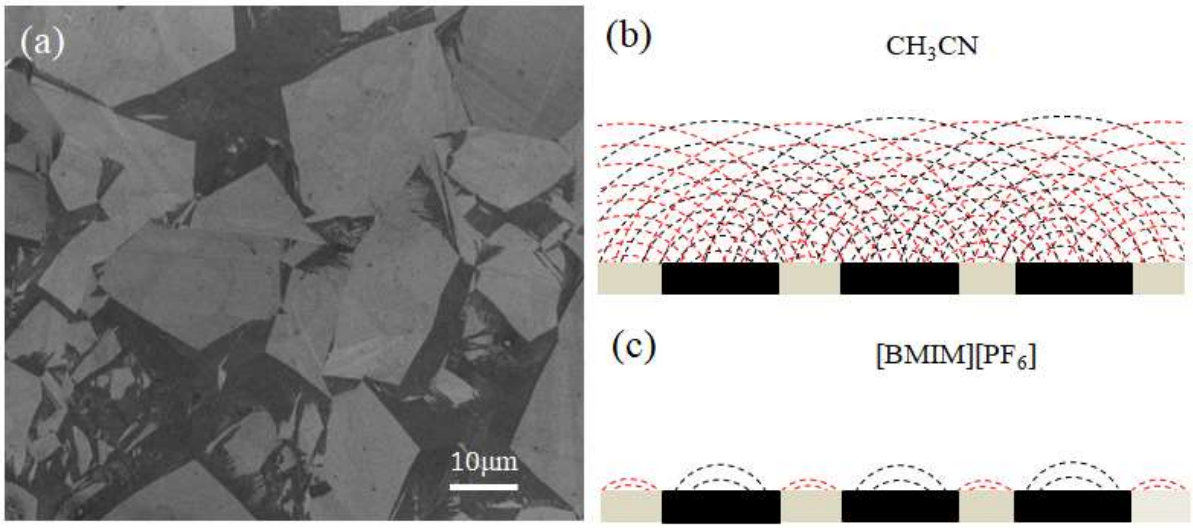

Figure 4. (a) An SEM image of the BDD electrode surface. Schematic representation of diffusion layers for Fc on the experimental timescale at a BDD electrode in (b) acetonitrile and (c) [BMIM][PF_6]. Black blocks represent surface facets with higher boron content giving higher k^0 values. Gray blocks represent lower boron content giving lower k^0 values. Noted that the diffusion layer thickness in (b) and (c) are for illustrative purposes only and are not drawn to scale.

Another explanation for the apparently frequency and harmonic dependent k^0 value is that there is a sp^2 carbon impurity present on the BDD electrode surface. Although the growth conditions for the BDD employed herein were selected to minimise sp^2 carbon content,[6, 8] an

sp^2 carbon-rich region is expected at the sidewalls of the BDD cylinder (cut from the wafer) introduced during the laser cutting process. While this region is initially encapsulated in the insulating glass sheath in which the BDD is mounted (*vide supra*), with polishing to reveal the electrode disk geometry and further polishing to clean the electrode, sidewall exposure is expected over time, as only glass will mechanical wear away during alumina polishing. As shown in the SI, Figure S13(a) and (b) shows a photograph and an optical micrograph, respectively, of an "overpolished" BDD electrode, where the BDD does indeed protrude from the surrounding glass sheath to expose the edge (sidewall) region, which is known to be rich in sp^2 carbon.

Raman spectroscopy was used to locally probe the sp^3 and sp^2 content at different areas of the BDD electrode surface. The Raman spectra shown in Figure 5a display the characteristic diamond bond associated with sp^3 carbon, at 1332 cm^{-1} for both the BDD electrode face (black) and edge (red). However, an additional band in the 1400 – 1600 cm^{-1} region, which corresponds to sp^2 carbon, is also present in the spectrum obtained from the edge of the BDD electrode (region indicated in Figure 5b with a black line).[6] Figure 5c illustrates the result of mapping the sp^2/sp^3 ratio across a line on the edge of BDD electrode (see black line in Figure 5b). Again, these Raman spectra confirm that there is a significant amount of sp^2 carbon present along the exposed edge of the BDD electrode. Since this exposed area of the electrode will be in contact with solution during the FTAC voltammetric measurement, it is highly likely that the $Fc^{0/+}$ process occurs at a different rates on the surrounding edge to that for the surface region of the BDD disk. Given the high viscosity of [BMIM][PF_6], and the consequently short diffusion length on the FTAC voltammetric timescale, these regions are expected to be largely diffusionally isolated from each other (Figure 4), leading to kinetic dispersion and an apparently harmonic-dependent k^0 value, as reported above.

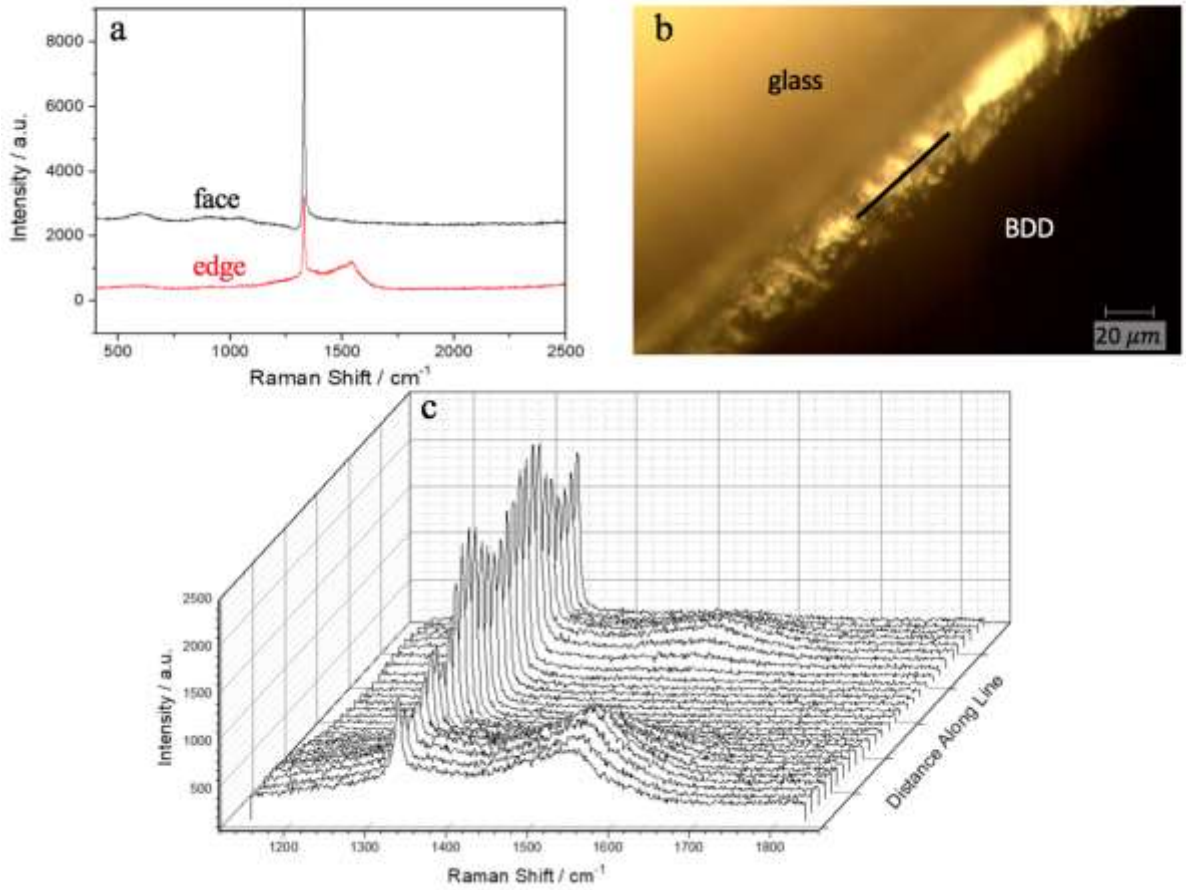

Figure 5. (a) Raman spectra of the face (black) and edge (red) of a BDD electrode. (b) Optical microscope image of the edge of a BDD electrode. The black line refers to the Raman mapping pathway. (c) Raman mapping as a function of distance along the line displayed in (b).

FTAC voltammetric analysis of the $Fc^{0/+}$ process in [BMIM][PF_6] at a BDD-wax electrode. If the kinetic dispersion is predominantly due to the exposed electrode edge, rather than spatial variations in boron levels, a significantly lower level of discrepancy between experimental and simulated data should be observed if this sp^2 carbon enriched region present at the edge of the BDD disk is removed. To test this hypothesis, an insulating wax mask containing a small hole in the middle was sealed onto the face of the BDD electrode, so that the edge of the electrode was no longer exposed electrochemically to the solution (SI, Figure S1). With this modified design, now referred to as a BDD-wax electrode, significantly improved agreement between experiment and theory based on a homogeneous surface was obtained for the $Fc^{0/+}$ process in [BMIM][PF_6] at all harmonics using frequencies of 9.02 Hz and 26.97 Hz (Figures 6 and SI, Figure S14) and a Fc concentration of 1.0 mM. Under these conditions, the optimized k^0 values

were determined to be 0.0015 cm^2 s^{-1} at both frequencies with LS values of 92.1% and 90.1%, respectively, much improved compared to that obtained at the non-waxed BDD electrode (LS = 83.2% and 74.0%) and indeed comparable to that obtained at a GC electrode, as summarized in Table 3. With a lower 0.50 mM concentration of Fc, experimental and simulated data are again in excellent agreement (SI, Figure S15 and S16 for f = 9.02 and 26.97 Hz, respectively), implying that the IR_u effect was correctly modelled and adsorption was insignificant.

Table 3 Comparison of k^0 values derived from experiment versus simulation comparison of $Fc^{0/+}$ processes in [BMIM][PF_6] at bare BDD and BDD-wax electrodes.

	Bare BDD		BDD-wax	
	9 Hz	27 Hz	9 Hz	27 Hz
k^0 (cm s^{-1})	0.0023	0.0025	0.0015	0.0015
LS (%)	83.2	74.0	92.1	90.1

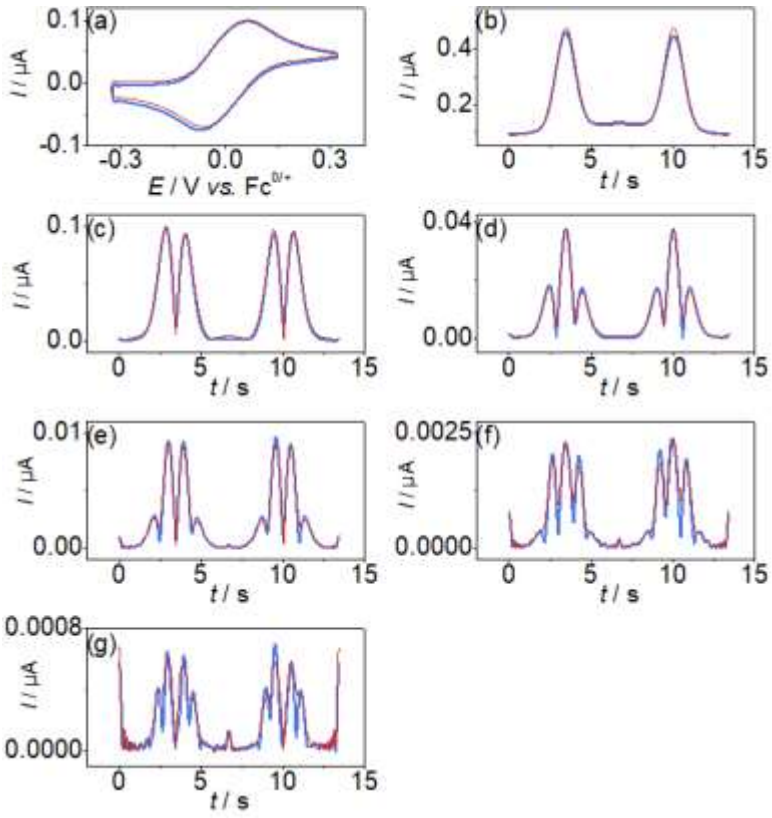

Figure 6. Comparison of simulated (red) and experimental (blue) FTAC voltammetric data obtained from the oxidation of 1.0 mM Fc in [BMIM][PF_6] at a BDD-wax electrode with ΔE = 80 mV, f = 9.02 Hz and v = 0.089 V s^{-1}. (a) aperiodic DC component, (b-g) 1st to 6th AC harmonic components. The simulation parameters are A = 5.7 × 10^{-3} cm^2, D = 6.3 × 10^{-8} cm^2 s^{-1}, R_u = 18510 Ω, E^0 = 0 V *vs.* $Fc^{0/+}$, C_{dl} (C_0 = 3.7, C_1 = 1.5, C_2 = 0.6, C_3 = -5.0, C_4 = 6.2) (see eq 2), T = 295 K, k^0 = 0.0015 cm s^{-1} and a = 0.50. LS = 92.1 %.

The substantial increase in LS when using a BDD-wax electrode strongly supports the hypothesis that the origin of most of the discrepancy is the contribution from sp^2 carbon-rich region at the edge of the BDD electrode, with the k^0 value at the sp^2 rich edge being much larger (see GC results above) than at pure BDD. As an approximation, it can be assumed that k^0 for the $Fc^{0/+}$ process in [BMIM][PF_6] on sp^2 carbon (structurally analogous to GC) and sp^3 BDD (waxed electrode) are 0.04 and 0.0015 cm s^{-1}, respectively. A large difference (1 to 2 orders of magnitude)[31] is needed to observe a significant deviation between the experimental FTAC voltammetric results and simulations that assume a uniformly active electrode surface. Given that the BDD-wax electrode is itself a heterogeneous surface (*i.e.*, polycrystalline) with facet-dependent kinetics,[9-11] the good experiment-theory agreement also implies that the difference between k^0 values on differently doped grains (see hypothesis one illustrated in Figure 4) is not be large enough to observe macroscopically, with FTAC voltammetry.

Comparison of electrode kinetics on pristine and micromachined (sp^2-rich) BDD using an electrochemical droplet cell. As a final test, a mobile electrochemical droplet cell[42-43] was employed to probe the structure-dependent electrode kinetics of the $Fc^{0/+}$ process on a polycrystalline BDD substrate (light areas in Figure 7a) to that possessed by a defined region of sp^2-rich material (black disk in Figure 7a). The disk-shaped (diameter = 400 μm) sp^2-rich area was introduced by laser micromachining,[22, 55] and simulates the edge-regions of the BDD macrodisk electrode employed in FTAC voltammetry (Figures 1 and 2). In the droplet cell format, localised DC cyclic voltammetric measurements were performed within confined areas of the electrode surface (*i.e.*, pristine BDD or sp^2-rich regions). The IL residue "footprint" shown in Figure 7a is, defined by the dimensions of the droplet (meniscus) formed at the end

of a pulled glass capillary (micropipet) having a diameter of ≈ 50 μm (Figure 7b) filled with the Fc in [BMIM][PF_6].

Localised DC cyclic voltammograms obtained on the pristine BDD and sp^2-rich area of the electrode surface are shown in Figure 7c-i and c-ii, respectively. Both DC cyclic voltammograms are peak-shaped, indicating that mass-transport occurs predominantly by planar (1D) diffusion, attributable to the large probe dimensions[56] and high viscosity of the IL electrolyte, leading to the low diffusion coefficient (*ca.* 6×10^{-8} cm^2 s^{-1}, *vide supra*) of Fc. There is a significant background (nonfaradaic) current contribution in the cyclic voltammograms, especially in the micromachined sp^2-rich area, and thus quantitative treatment of these data has not been attempted here. Nevertheless, the large voltammetric peak-to-peak separations, ΔE_p, obtained on the pristine BDD surface (Figure 7c-i, $\Delta E_p > 150$ mV) compared to the laser micromachined sp^2-rich area, where ΔE_p is close to that predicted for an ideal, electrochemically reversible process (Figure 7c-ii, $\Delta E_p \approx 70$ mV) qualitatively indicates that the kinetics of the $Fc^{0/+}$ process are more facile on the latter surface, confirming the FTAC voltammetry results, above.

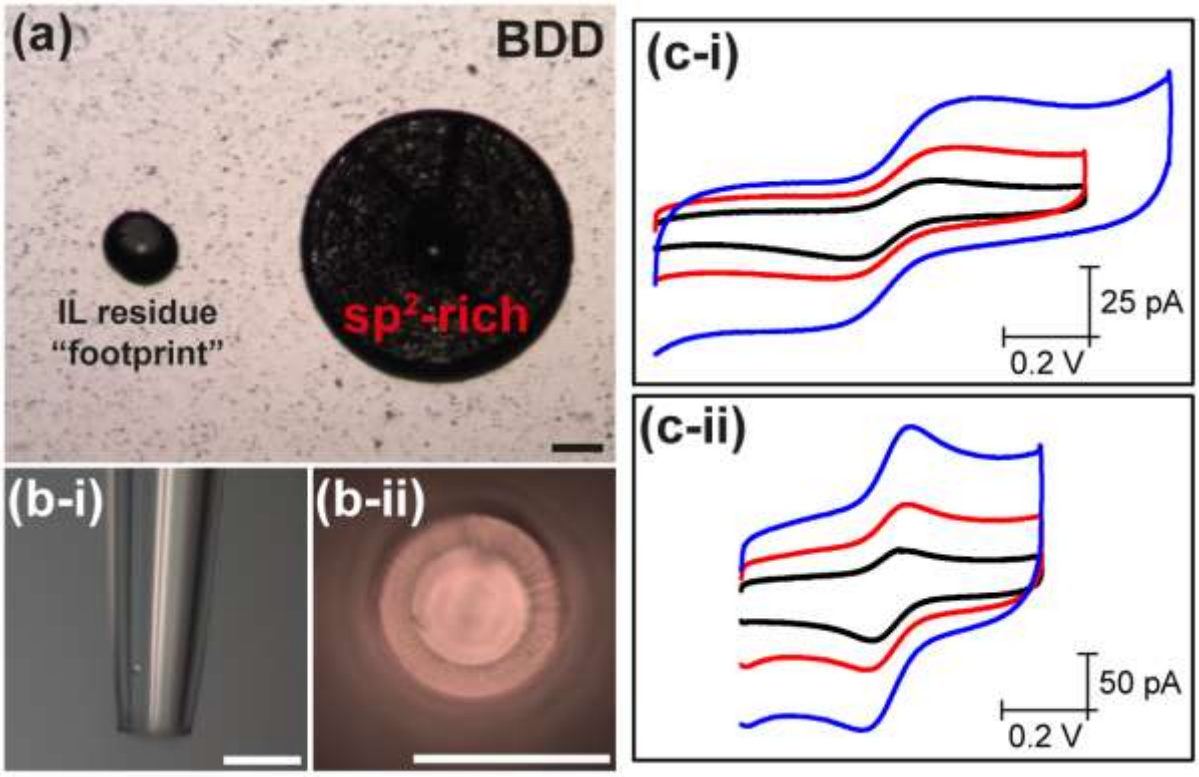

Figure 7. Localised voltammetric measurements performed in the electrochemical droplet cell format on a polycrystalline BDD surface that possesses a segregated area of sp^2-rich material, introduced by laser micromachining. **(a)** Optical micrograph of the machined BDD surface, post-measurement (the IL residue "footprint" is labelled). **(b)** Optical micrographs of the **(i)** side and **(ii)** end of the micropipet probe (diameter ≈ 50 μm) used to form the electrochemical microdroplet cell. The scale bar indicates 75 μm in (a-b). **(c)** DC cyclic voltammograms obtained from the oxidation of 3.4 mM Fc in [BMIM][PF_6] at the **(i)** pristine BDD and **(ii)** laser micromachined (sp^2-rich) areas of the electrode surface, with voltammetric scan rates, ν = 10, 25 and 50 mV s^{-1} (black, red and blue traces, respectively). Note the differing current scales in (c-i) and (c-ii).

CONCLUSIONS

In this work, the effect of a sp^2 carbon-rich edge surrounding BDD disk electrodes was investigated through a combination of FTAC voltammetry, microscopy and Raman spectroscopy. With sp^2 carbon-rich regions at the edge and predominantly sp^3 carbon on the face of BDD disk electrodes, FTAC voltammetric data imply kinetic dispersion is asscoaited with the oxidation of Fc in highly viscous [BMIM][PF_6]. Thus, poor agreement between theory and experiment was found using a model that assumes a homogeneous surface and Butler-Volmer electrode kinetics. However, upon physically blocking the edge of the electrode so that only the face of the BDD was exposed, far superior agreement between experimental and simulated data was achieved assuming a uniformly active electrode surface, with a k^0 value of

0.0015 cm s^{-1}. Localised voltammetric measurements performed with an electrochemical droplet cell confirmed that the sp^2 carbon-rich regions exhibit much faster electron transfer kinetics for the $Fc^{0/+}$ process in [BMIM][PF_6] than the sp^3 BDD surface.

In summary, this work demonstrates that sp^2 carbon impurities can significantly affect the electrochemical behaviour of BDD electrodes, especially under conditions of slow mass transport and short experimental timescales, such that individual sp^2 and sp^3 regions respond individually, rather than collectively. Furthermore, it is demonstrated that FTAC voltammetry allows spatial variations in electrode activity to be identified under these conditions.

ASSOCIATED CONTENT

SUPPORTING INFORMATION

Procedure for the preparation of the BDD-wax electrode, determination of diffusion coefficient, estimation of the radial diffusion contribution on the DC voltammetric timescale, photographs of an "overpolished" BDD electrode (Figure S13), and additional FTAC voltammetric data (Figures S2-S7, S9-S12 and S14-S16).

ACKNOWLEDGMENTS

The authors gratefully acknowledge the Australian Research Council for financial support. C.L.B. acknowledges financial support from the Ramsay Memorial Fellowship Trust. J.V.M acknowledges the Royal Society for an Industry Fellowship (INF/R1/180026). S.J.C acknowledges the Centre for Doctoral Training in Diamond Science and Technology (EP/ L015315/1) with the Defence Science and Technology Laboratory (Dstl). P.R.U. thanks the Royal Society for a Wolfson Research Merit Award. We are grateful for support from the Monash-Warwick Alliance (studentship for S.-y.T.).

REFERENCES

1. McCreery, R. L., Advanced Carbon Electrode Materials for Molecular Electrochemistry. *Chem. Rev.* **2008**, *108*, 2646-2687.
2. Sarada, B.; Rao, T. N.; Tryk, D.; Fujishima, A., Electrochemical Oxidation of Histamine and Serotonin at Highly Boron-Doped Diamond Electrodes. *Anal. Chem.* **2000**, *72*, 1632-1638.
3. Moiroux, J.; Elving, P. J., Effects of Adsorption, Electrode Material, and Operational Variables on the Oxidation of Dihydronicotinamide Adenine Dinucleotide at Carbon Electrodes. *Anal. Chem.* **1978**, *50*, 1056-1062.
4. Balmer, R.; Brandon, J.; Clewes, S.; Dhillon, H.; Dodson, J.; Friel, I.; Inglis, P.; Madgwick, T.; Markham, M.; Mollart, T., Chemical Vapour Deposition Synthetic Diamond: Materials, Technology and Applications. *J. Phys.: Condens. Matter* **2009**, *21*, 364221.
5. Pleskov, Y. V., Electrochemistry of Diamond: A Review. *Russ. J. Electrochem.* **2002**, *38*, 1275-1291.
6. Macpherson, J. V., A Practical Guide to Using Boron Doped Diamond in Electrochemical Research. *Phys. Chem. Chem. Phys.* **2015**, *17*, 2935-2949.
7. Granger, M. C.; Witek, M.; Xu, J.; Wang, J.; Hupert, M.; Hanks, A.; Koppang, M. D.; Butler, J. E.; Lucazeau, G.; Mermoux, M., Standard Electrochemical Behavior of High-Quality, Boron-Doped Polycrystalline Diamond Thin-Film Electrodes. *Anal. Chem.* **2000**, *72*, 3793-3804.
8. Hutton, L. A.; Iacobini, J. G.; Bitziou, E.; Channon, R. B.; Newton, M. E.; Macpherson, J. V. J., Examination of the Factors Affecting the Electrochemical Performance of Oxygen-Terminated Polycrystalline Boron-Doped Diamond Electrodes. *Anal. Chem.* **2013**, *85*, 7230-7240.
9. Tomlinson, L. I.; Patten, H. V.; Green, B. L.; Iacobini, J.; Meadows, K. E.; McKelvey, K.; Unwin, P. R.; Newton, M. E.; Macpherson, J. V., Intermittent- Contact Scanning Electrochemical Microscopy (IC-SECM) as a Quantitative Probe of Defects in Single Crystal Boron Doped Diamond Electrodes. *Electroanalysis* **2016**, *28*, 2297-2302.
10. Patten, H. V.; Meadows, K. E.; Hutton, L. A.; Iacobini, J. G.; Battistel, D.; McKelvey, K.; Colburn, A. W.; Newton, M. E.; Macpherson, J. V.; Unwin, P. R., Electrochemical Mapping Reveals Direct Correlation between Heterogeneous Electron - Transfer Kinetics and Local Density of States in Diamond Electrodes. *Angew. Chem., Int. Ed.* **2012**, *51*, 7002-7006.
11. Patten, H. V.; Lai, S. C.; Macpherson, J. V.; Unwin, P. R., Active Sites for Outer-Sphere, Inner-Sphere, and Complex Multistage Electrochemical Reactions at Polycrystalline Boron-Doped Diamond Electrodes (pBDD) Revealed with Scanning Electrochemical Cell Microscopy (SECCM). *Anal. Chem.* **2012**, *84*, 5427-5432.
12. Zhang, J.; Guo, S.-X.; Bond, A. M.; Marken, F., Large-Amplitude Fourier Transformed High-Harmonic Alternating Current Cyclic Voltammetry: Kinetic Discrimination of Interfering Faradaic Processes at Glassy Carbon and at Boron-Doped Diamond Electrodes. *Anal. Chem.* **2004**, *76*, 3619-3629.
13. Amatore, C.; Savéant, J. M.; Tessier, D., Charge Transfer at Partially Blocked Surfaces: A Model for the Case of Microscopic Active and Inactive Sites. *J. Electroanal. Chem. Interfacial Electrochem.* **1983**, *147*, 39-51.
14. Bennett, J. A.; Wang, J.; Show, Y.; Swain, G. M., Effect of sp2-Bonded Nondiamond Carbon Impurity on the Response of Boron-Doped Polycrystalline Diamond Thin-Film Electrodes. *J. Electrochem. Soc.* **2004**, *151*, E306-E313.
15. Ayres, Z. J.; Newland, J. C.; Newton, M. E.; Mandal, S.; Williams, O. A.; Macpherson, J. V., Impact of Chemical Vapour Deposition Plasma Inhomogeneity on the Spatial Variation of sp2 Carbon in Boron Doped Diamond Electrodes. *Carbon* **2017**, *121*, 434-442.

16. Duo, I.; Fujishima, A.; Comninellis, C., Electron Transfer Kinetics on Composite Diamond (sp3)–Graphite (sp2) Electrodes. *Electrochem. Commun.* **2003**, *5*, 695-700.
17. Williams, O., Nanocrystalline Diamond. *Diamond Relat. Mater.* **2011**, *20*, 621-640.
18. Yang, N.; Yu, S.; Macpherson, J. V.; Einaga, Y.; Zhao, H.; Zhao, G.; Swain, G. M.; Jiang, X., Conductive Diamond: Synthesis, Properties, and Electrochemical Applications. *Chem. Soc. Rev.* **2019**, *48*, 157-204.
19. Wilson, N. R.; Clewes, S. L.; Newton, M. E.; Unwin, P. R.; Macpherson, J. V., Impact of Grain-Dependent Boron Uptake on the Electrochemical and Electrical Properties of Polycrystalline Boron Doped Diamond Electrodes. *J. Phys. Chem. B* **2006**, *110*, 5639-5646.
20. Hutton, L. A.; Iacobini, J. G.; Bitziou, E.; Channon, R. B.; Newton, M. E.; Macpherson, J. V., Examination of the Factors Affecting the Electrochemical Performance of Oxygen-Terminated Polycrystalline Boron-Doped Diamond Electrodes. *Anal. Chem.* **2013**, *85*, 7230-7240.
21. Hutton, L.; Newton, M. E.; Unwin, P. R.; Macpherson, J. V., Amperometric Oxygen Sensor Based on a Platinum Nanoparticle-Modified Polycrystalline Boron Doped Diamond Disk Electrode. *Anal. Chem.* **2008**, *81*, 1023-1032.
22. Ayres, Z. J.; Cobb, S. J.; Newton, M. E.; Macpherson, J. V., Quinone Electrochemistry for the Comparative Assessment of Sp2 Surface Content of Boron Doped Diamond Electrodes. *Electrochem. Commun.* **2016**, *72*, 59-63.
23. Tania L. R.; Samuel J. C.; Macpherson J. V., An sp2 Patterned Boron Doped Diamond Electrode for the Simultaneous Detection of Dissolved Oxygen and pH. *ACS Sens.* **2019**, *4*, 756-763
24. Cobb, S. J.; Ayres, Z. J.; Newton, M. E.; Macpherson, J. V., Deconvoluting Surface-Bound Quinone Proton Coupled Electron Transfer in Unbuffered Solutions: Toward a Universal Voltammetric pH Electrode. *J. Am. Chem. Soc.* **2018**, *141*, 1035-1044.
25. Streeter, I.; Baron, R.; Compton, R. G., Voltammetry at Nanoparticle and Microparticle Modified Electrodes: Theory and Experiment. *J. Phys. Chem. C* **2007**, *111*, 17008-17014.
26. Ray, K.; McCreery, R. L., Spatially Resolved Raman Spectroscopy of Carbon Electrode Surfaces: Observations of Structural and Chemical Heterogeneity. *Anal. Chem.* **1997**, *69*, 4680-4687.
27. Compton, R. G.; Banks, C. E., *Understanding Voltammetry*; World Scientific, 2011.
28. Cinková, K.; Batchelor-McAuley, C.; Marton, M.; Vojs, M.; Švorc, Ľ.; Compton, R. G., The Activity of Non-Metallic Boron-Doped Diamond Electrodes with Sub-Micron Scale Heterogeneity and the Role of the Morphology of sp2 Impurities. *Carbon* **2016**, *110*, 148-154.
29. Duo, I.; Fujishima, A.; Comninellis, C., Electron Transfer Kinetics on Composite Diamond (sp3)–Graphite (sp2) Electrodes. *Electrochem. Commun.* **2003**, *5*, 695-700.
30. Davies, T. J.; Moore, R. R.; Banks, C. E.; Compton, R. G., The Cyclic Voltammetric Response of Electrochemically Heterogeneous Surfaces. *J. Electroanal. Chem.* **2004**, *574*, 123-152.
31. Tan, S.-y.; Unwin, P. R.; Macpherson, J. V.; Zhang, J.; Bond, A. M., Probing Electrode Heterogeneity Using Fourier-Transformed Alternating Current Voltammetry: Application to a Dual-Electrode Configuration. *Anal. Chem.* **2017**, *89*, 2830-2837.
32. Bentley, C. L.; Li, J.; Bond, A. M.; Zhang, J., Mass-Transport and Heterogeneous Electron-Transfer Kinetics Associated with the Ferrocene/Ferrocenium Process in Ionic Liquids. *J. Phys. Chem. C* **2016**, *120*, 16516-16525.
33. Rogers, E. I.; Silvester, D. S.; Poole, D. L.; Aldous, L.; Hardacre, C.; Compton, R. G., Voltammetric Characterization of the Ferrocene| Ferrocenium and Cobaltocenium| Cobaltocene Redox Couples in Rtils. *J. Phys. Chem. C* **2008**, *112*, 2729-2735.

34. Matsumiya, M.; Terazono, M.; Tokuraku, K., Temperature Dependence of Kinetics and Diffusion Coefficients for Ferrocene/Ferricenium in Ammonium-Imide Ionic Liquids. *Electrochim. Acta* **2006**, *51*, 1178-1183.
35. Zhao, C.; Bond, A. M.; Compton, R. G.; O'Mahony, A. M.; Rogers, E. I., Modification and Implications of Changes in Electrochemical Responses Encountered When Undertaking Deoxygenation in Ionic Liquids. *Anal. Chem.* **2010**, *82*, 3856-3861.
36. Bond, A. M.; Duffy, N. W.; Guo, S.-X.; Zhang, J.; Elton, D., Changing the Look of Voltammetry. *Anal. Chem.* **2005**, *77*, 186A-195A
37. Guo, S.-X.; Bond, A. M.; Zhang, J., Fourier Transformed Large Amplitude Alternating Current Voltammetry: Principles and Applications. *Rev. Polarogr.* **2015**, *61*, 21-32.
38. Bond, A. M.; Elton, D.; Guo, S.-X.; Kennedy, G. F.; Mashkina, E.; Simonov, A. N.; Zhang, J., An Integrated Instrumental and Theoretical Approach to Quantitative Electrode Kinetic Studies Based on Large Amplitude Fourier Transformed Ac Voltammetry: A Mini Review. *Electrochem. Commun.* **2015**, *57*, 78-83.
39. Gritzner, G.; Kuta, J., Recommendations on Reporting Electrode Potentials in Nonaqueous Solvents (Recommendations 1983). *Pure Appl. Chem.* **1984**, *56*, 461-466.
40. Bard, A. J.; Faulkner, L. R., Fundamentals and Applications. *Electrochemical Methods*, New York: wiley, **2001**.
41. Wang, Y.; Rogers, E. I.; Compton, R. G., The Measurement of the Diffusion Coefficients of Ferrocene and Ferrocenium and Their Temperature Dependence in Acetonitrile Using Double Potential Step Microdisk Electrode Chronoamperometry. *J Electroanal. Chem.* **2010**, *648*, 15-19.
42. Ebejer, N.; Güell, A. G.; Lai, S. C. S.; McKelvey, K.; Snowden, M. E.; Unwin, P. R., Scanning Electrochemical Cell Microscopy: A Versatile Technique for Nanoscale Electrochemistry and Functional Imaging. *Annu. Rev. Anal. Chem.* **2013**, *6*, 329-351.
43. Bentley, C. L.; Kang, M.; Unwin, P. R., Scanning Electrochemical Cell Microscopy: New Perspectives on Electrode Processes in Action. *Curr. Opin. Electrochem.* **2017**, *6*, 23-30.
44. Li, J.; Kennedy, G. F.; Bond, A. M.; Zhang, J., Demonstration of Superiority of the Marcus–Hush Electrode Kinetic Model in the Electrochemistry of Dissolved Decamethylferrocene at a Gold-Modified Electrode by Fourier-Transformed Alternating Current Voltammetry. *J. Phys. Chem. C* **2018**, *122*, 9009-9014.
45. Bond, A. M.; Duffy, N. W.; Elton, D. M.; Fleming, B. D., Characterization of Nonlinear Background Components in Voltammetry by Use of Large Amplitude Periodic Perturbations and Fourier Transform Analysis. *Anal. Chem.* **2009**, *81*, 8801-8808.
46. Kennedy, G. F.; Bond, A. M.; Simonov, A. N., Modelling Ac Voltammetry with Mecsim: Facilitating Simulation–Experiment Comparisons. *Curr. Opin. Electrochem.* **2017**, *1*, 140-147.
47. Haymond, S.; Babcock, G. T.; Swain, G. M., Electron Transfer Kinetics of Ferrocene at Microcrystalline Boron- Doped Diamond Electrodes: Effect of Solvent and Electrolyte. *Electroanalysis* **2003**, *15*, 249-253.
48. Suffredini, H. B.; Pedrosa, V. A.; Codognoto, L.; Machado, S. A.; Rocha-Filho, R. C.; Avaca, L. A., Enhanced Electrochemical Response of Boron-Doped Diamond Electrodes Brought on by a Cathodic Surface Pre-Treatment. *Electrochim. Acta* **2004**, *49*, 4021-4026.
49. Alehashem, S.; Chambers, F.; Strojek, J. W.; Swain, G. M.; Ramesham, R., Cyclic Voltammetric Studies of Charge Transfer Reactions at Highly Boron-Doped Polycrystalline Diamond Thin-Film Electrodes. *Anal. Chem.* **1995**, *67*, 2812-2821.
50. Dekanski, A.; Stevanović, J.; Stevanović, R.; Nikolić, B. Ž.; Jovanović, V. M., Glassy Carbon Electrodes: I. Characterization and Electrochemical Activation. *Carbon* **2001**, *39*, 1195-1205.

51. Nagaoka, T.; Yoshino, T., Surface Properties of Electrochemically Pretreated Glassy Carbon. *Anal. Chem.* **1986**, *58*, 1037-1042.
52. Swain, G. M., Solid Electrode Materials: Pretreatment and Activation. *Handbook of Electrochemistry*, Elsevier: Amsterdam, **2007**.
53. Harris, P. J. F., Fullerene-Related Structure of Commercial Glassy Carbons. *Philos. Mag.* **2004**, *84*, 3159-3167.
54. Fleming, B. D.; Zhang, J.; Bond, A. M.; Bell, S. G.; Wong, L.-L., Separation of Electron-Transfer and Coupled Chemical Reaction Components of Biocatalytic Processes Using Fourier Transform Ac Voltammetry. *Anal. Chem.* **2005**, *77*, 3502-3510.
55. Ayres, Z. J.; Borrill, A. J.; Newland, J. C.; Newton, M. E.; Macpherson, J. V., Controlled Sp2 Functionalization of Boron Doped Diamond as a Route for the Fabrication of Robust and Nernstian pH Electrodes. *Anal. Chem.* **2015**, *88*, 974-980.
56. Snowden, M. E.; Güell, A. G.; Lai, S. C. S.; McKelvey, K.; Ebejer, N.; O'Connell, M. A.; Colburn, A. W.; Unwin, P. R., Scanning Electrochemical Cell Microscopy: Theory and Experiment for Quantitative High Resolution Spatially-Resolved Voltammetry and Simultaneous Ion-Conductance Measurements. *Anal. Chem.* **2012**, *84*, 2483-2491.

TOC graphic: